Journal of Alloys and Compounds 639 (2015) 9–14

Contents lists available at ScienceDirect

Journal of Alloys and Compounds

journal homepage: www.elsevier.com/locate/jalcom

# Enhanced thermoelectric performance of n-type $Bi_2Se_3$ doped with Cu

Guolong Sun [a,b], Xiaoying Qin [b,*], Di Li [b], Jian Zhang [b], Baojin Ren [b], Tianhua Zou [b], Hongxing Xin [b], Silke Buehler Paschen [c], Xinlin Yan [c]

[a] School of Physics and Materials Science, Anhui University, Hefei 230039, PR China
[b] Key Laboratory of Materials Physics, Institute of Solid State Physics, Chinese Academy of Sciences, 230031 Hefei, PR China
[c] Institute of Solid State Physics, Vienna University of Technology, Wiedner Hauptstr. 8-10, 1040 Vienna, Austria

ARTICLE INFO

*Article history:*
Received 2 December 2014
Received in revised form 11 March 2015
Accepted 15 March 2015
Available online 21 March 2015

*Keywords:*
Thermoelectric performance
$Bi_2Se_3$
Thermal conductivity

ABSTRACT

The thermoelectric properties of Cu-doped $Cu_xBi_2Se_3$ ($x = 0$, 0.005, 0.010, 0.015 and 0.020) were investigated in the temperature range of 300 K to 590 K. The results indicate that, at 300 K, the thermal conductivity of moderately doped $Cu_xBi_2Se_3$ ($x = 0.010$ and 0.015) is by 30–50% lower than that of un-doped $Bi_2Se_3$, which is attributed to enhanced phonon scattering by the dopant. Though the absolute values of the thermopower are reduced by the doping, the electrical resistivity of the doped samples is strongly reduced (by ~30% at 500 K, for instance), thus maintaining high values of power factor at both 300 K and 590 K, especially for samples with $x \geqslant 0.01$. As a result, the lightly doped compound $Cu_{0.01}Bi_2Se_3$ exhibits the best thermoelectric performance, with a figure of merit, ZT, of 0.54 at 590 K. This is more than twice larger than that of the un-doped $Bi_2Se_3$ studied here, suggesting that proper Cu-doping in $Bi_2Se_3$ is a promising way to improve its thermoelectric performance.



## 1. Introduction

Thermoelectric materials have attracted tremendous attention for their ability to convert energies between heat and electricity directly [1,2]. The efficiency of thermoelectric materials can be characterized by a dimensionless figure of merit that is defined as: $ZT = S^2\sigma T/\kappa$, where $S$, $\sigma$, $\kappa$, and $T$ are Seebeck coefficient, electrical conductivity, thermal conductivity and temperature, respectively [3–5]. Therefore, large $\sigma$, large $S$ and small $\kappa$ should be achieved at the same time for a good thermoelectric material. The alloys of V–VI binary compounds, such as $Bi_2Te_3$ [2,3,6,7], $Sb_2Te_3$ [8,9] and $Bi_2Se_3$ [10,11] and ternary compounds, e.g. $Bi_2Te_{1-x}Se_x$ [12–16] and $Bi_xSb_{1-x}Te_3$ [17–19], are the best candidates of high-efficient thermoelectric materials. Among these binary isostructural compounds, $Bi_2Se_3$ has received much attention recently due to its relatively large band-gap ($E_g = 0.3$ eV), which makes it be suitable for utilization near or above room temperatures. Recent theoretical studies show that $Bi_2Se_3$ is one of the most promising thermoelectric materials [10,20–22]. Experimentally, $Bi_2Se_3$ nanostructures were synthesized by Kadel et al. and a maximum value of $ZT = 0.096$ was obtained at 523 K [23]. Hor et al. studied the thermoelectric properties of *p*-type $Bi_2Se_3$ single crystals in the temperature range from 2 K to 300 K, and they obtained a highest $ZT = 0.17$ at 300 K [24]. Thermoelectric properties of $Bi_2Se_3$ nanoflakes were studied by Min et al., and a maximum $ZT = \sim 0.19$ at 480 K was achieved [25]. Recently, Sun et al. obtained a ZT value of 0.35 at 400 K for $Bi_2Se_3$ single-layer based composites, which is ca. 8 times higher than that of the bulk material [26]. Nonetheless, the reported ZT values of $Bi_2Se_3$ are still too small to meet the requirements of practical applications. Hence, it is imperative to further optimize its thermoelectric performance.

$Bi_2Se_3$ has a rhombohedral layered structure which is based on slabs of five shifted Se and Bi atomic layers stacked along the *c*-axis. Adjacent $Se^{(2)}$–$Se^{(2)}$ atomic layers are bound by van der Waals faces. This is similar to the layer-structured $TiS_2$ [27] where the van der Waals gap allows for intercalation by a wide range of both organic and inorganic materials [28,29] and leads to the reduction of the thermal conductivity and an improvement of the thermoelectric performance [30,31]. Hence, the introduction (doping) of guest atoms into the van der Waals gap of $Bi_2Se_3$ appears as promising way to enhance the thermoelectric performance.

Previous work revealed that copper can intercalate into the van der Waals gap of $Bi_2Se_3$ [32]. The Cu-doped compound $Cu_xBi_2Se_3$ ($0.12 \leqslant x \leqslant 0.15$) is found to exhibit superconductivity at low temperatures (3.8 K) [33]. However, the high-temperature thermoelectric properties of $Cu_xBi_2Se_3$ have not been studied systematically. In this work, we prepared bulk samples of $Cu_xBi_2Se_3$ with different Cu contents ($x = 0$, 0.005, 0.010, 0.015 and 0.020) and studied their

* Corresponding author. Tel.: +86 0551 65592750; fax: +86 0551 65591434.
*E-mail address:* xyqin@issp.ac.cn (X. Qin).

http://dx.doi.org/10.1016/j.jallcom.2015.03.124
0925-8388/

thermoelectric properties in the temperature range from 300 K to 590 K. Our results show that the thermal conductivity of the moderately doped $Cu_xBi_2Se_3$ samples ($x = 0.010$, 0.015) is remarkably reduced; at the same time, the electrical resistivity is sizably decreased. Consequently, these doped compounds exhibit excellent thermoelectric performance. The largest ZT of about 0.54 at 590 K is obtained for $Cu_{0.01}Bi_2Se_3$.

## 2. Experimental section

$Cu_xBi_2Se_3$ ($x = 0$, 0.005, 0.010, 0.015, 0.020) compounds were synthesized by melting and hot-pressing method. The elements Cu (99.9%), Bi (99.999%) and Se (99.99%) were weighed in stoichiometric ratios, and were evacuated and sealed in a quartz ampule. The samples were placed in a digitally controlled furnace and heated slowly (20 K/h, about 2700 min) from room temperatures to 1073 K, held there for 12 h, and then cooled to 300 K naturally. The obtained compounds were ground to fine powders in agate mortar, and then compacted by vacuum hot pressing with the temperature 563 K and pressure 300 MPa for 60 min. The phase structures of the bulk samples were checked by X-ray diffraction (XRD) using a Philips X'Pert PRO X-ray diffractometer equipped with graphite monochromatic Cu Kα radiation ($\lambda = 1.54056$ Å). The morphology and the compositions were characterized by field emission scanning electron microscopy (FESEM) and energy dispersive X-ray spectroscopy (EDS) (Hitachi SU8020). Bars of $2 \times 2 \times 6$ mm$^3$ and disks of diameters of about 6–10 mm were cut and polished from the hot-pressed bulk disks for electronic- and thermal-transport measurements, which were performed on the commercial equipment ZEM-3(M08) (Ulvac Riko, Inc.) and the Netzsch LFA-457 system, respectively. All the thermoelectric properties were measured perpendicular to the hot pressing direction. The sample densities $D$ measured by the Archimedes' method were about 6.77–6.95 g cm$^{-3}$ (see in Table 1). The resulting thermal conductivity $\kappa$ was calculated from the measured thermal diffusivity $\alpha$, specific heat $C_p$, and density $D$ using the relationship $\kappa = \alpha D C_p$.

## 3. Results and discussion

### 3.1. Microstructure characteristics

The phase composition of the hot pressed bulk samples was checked by XRD, as shown in Fig. 1. It is clear that all the diffraction patterns can be indexed to $Bi_2Se_3$, in good agreement with the ICDD PDF number 00-033-0214. No other phase could be detected from the XRD patterns, which indicates that the Cu doped specimens have the same crystallographic structure as the $Bi_2Se_3$ phase. As is known, $Bi_2Se_3$ has a layered structure with the quintuple layer (QL) stacked along the $c$ axis with weak van der Waals interactions between neighboring QLs [34]. In order to identify the location of trace amounts of Cu, the values of the lattice parameters $a$ and $c$ for the doped samples were calculated from the XRD data and are presented in Fig. 2. It can be seen that the lattice parameter $c$ increases monotonously from 28.645 Å to 28.710 Å as the Cu content $x$ increases from 0.005 to 0.020. The lattice parameter $a$ does not show an appreciable change for $x \leqslant 0.015$; for $x = 0.020$ $a$ is slightly smaller. Obviously, the monotonous increase of $c$ with increasing $x$ suggests that Cu atoms are intercalated into the van der Waals gaps between QLs of $Bi_2Se_3$. The slight shrinkage of $a$ in the most heavily doped sample ($x = 0.020$) could arise from the requirements of lowing the distortion energy of the lattice, for large expansion of the lattice cells gives rise to high strain energy.

**Table 1**
Density $D$, relative density $D_r$, porosity $\Phi$, orientation factor $\gamma$ and the weight percent of Se and Bi of all $Cu_xBi_2Se_3$ samples with different Cu content $x$ studied here.

| $x$ | $D$ (g cm$^{-3}$) | $D_r$ (%) | $\Phi$ (%) | $\gamma$ | Se (wt%) | Bi (wt%) |
|---|---|---|---|---|---|---|
| 0 | 6.95 | 90.5 | 9.5 | 0.33 | 36.5 | 63.5 |
| 0.005 | 6.90 | 89.8 | 10.2 | 0.28 | 37.2 | 62.7 |
| 0.010 | 6.77 | 88.1 | 11.9 | 0.29 | 35.1 | 64.9 |
| 0.015 | 6.84 | 89.1 | 10.9 | 0.30 | 35.8 | 64.2 |
| 0.020 | 6.93 | 90.3 | 9.7 | 0.33 | 36.9 | 63.1 |

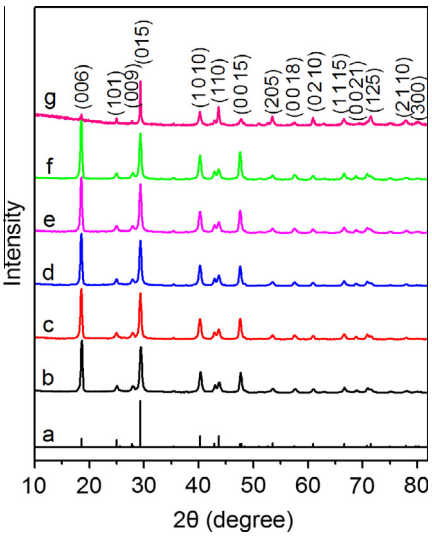


**Fig. 1.** XRD patterns of (a) ICDD PDF number 00-033-0214, (b–f) the $Cu_xBi_2Se_3$ bulk samples perpendicular to the hot pressing direction with the Cu contents $x = 0$, 0.005, 0.010, 0.015 and 0.020, respectively; (g) the $Cu_{0.015}Bi_2Se_3$ bulk sample parallel to the hot pressing direction.

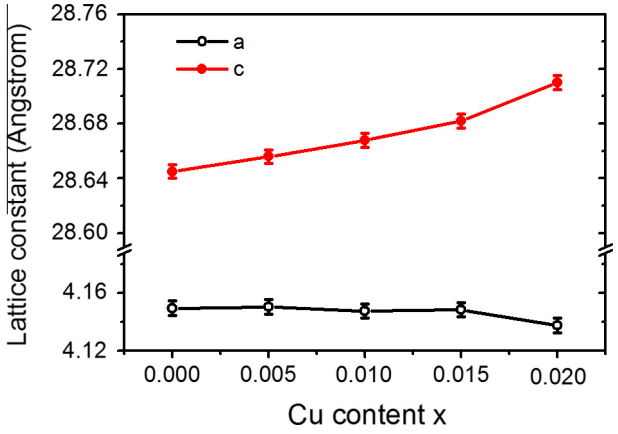


**Fig. 2.** Lattice constants $a$ and $c$ for the $Cu_xBi_2Se_3$ samples with the Cu contents $x = 0$, 0.005, 0.010, 0.015 and 0.020.

In addition, one notices from the XRD patterns that the intensity of the (00$l$) diffraction peaks for the doped samples perpendicular to the hot-pressing direction increases as compared with that of the (00$l$) peaks in the ICDD PDF number 00-033-0214, indicating that all of the samples have a preferred orientation due to the flake-like grains (also see Fig. 3) parallel to the [001] crystal planes of $Bi_2Se_3$. Quantitatively, the preferred orientation can be described by an orientation factor, defined as $\gamma = (P - P_0)/(1 - P_0)$, where $P$ is the fractional intensity of the (00$l$) planes, $P_0$ is the value of $P$ in the case of ideal isotropy and $P = \Sigma I(00l)/\Sigma I(hkl)$ [35]. The calculated $\gamma = 0.28$–$0.33$ for the $Cu_xBi_2Se_3$ samples of different Cu contents are given in Table 1. Sections parallel to the hot pressing direction have also been measured; the (00$l$) plane orientation factor measured in this direction is smaller than zero ($\gamma = \sim -0.1$), which is understandable since most of the grains have the (00$l$) plane lying in the plane normal to hot pressing direction, as shown in Fig. 3(f)–(j).

The microstructures of both the sections parallel and perpendicular to the hot pressing direction for the as-prepared bulk samples are characterized by field emission scanning electron microscopy (FESEM), as shown in Fig. 3. By comparing Fig. 3(a)–(e)

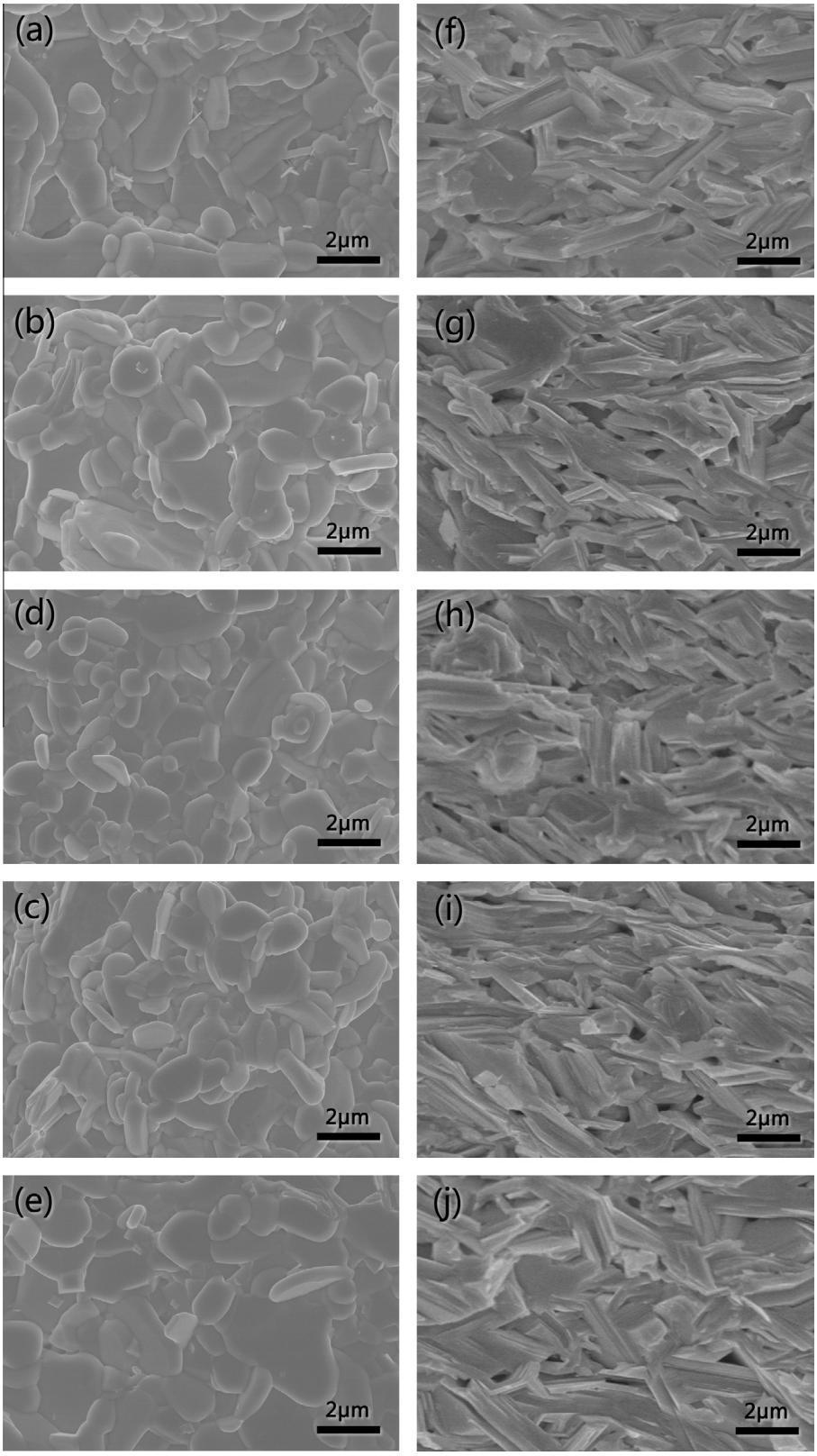


**Fig. 3.** FESEM images of the fracture surfaces ((a)–(e) perpendicular to and (f)–(j) parallel to the hot-pressing direction) of $Cu_xBi_2Se_3$ bulk samples for the different Cu contents $x$ = 0, 0.005, 0.010, 0.015 and 0.020, respectively.

with Fig. 3(f)–(j) we see that the grains observed in the sections perpendicular to the hot pressing direction show flake-like shape while the grains in the sections parallel to the hot-pressing direction show stripe-like shape, which agrees well with the measured orientation factors (Table 1). The average grain size perpendicular to the hot-pressing direction Fig. 3(a)–(e) does not change substantially from sample to sample. It is measured to be around 0.89 μm, 0.91 μm, 0.90 μm, 0.90 μm and 0.91 μm for the $Cu_xBi_2Se_3$ samples

with $x = 0$, 0.005, 0.010, 0.015 and 0.020, respectively. Some much large grains are found in the heavily doped samples. The mean grain thickness observed parallel to the hot-pressing direction is about 0.26 μm for all the samples (Fig. 3(f)–(j)).

### 3.2. Transport properties

Fig. 4 shows the electrical resistivity $\rho$ of all $Cu_xBi_2Se_3$ samples ($x = 0$, 0.005, 0.010, 0.015, 0.020) with the temperature ranging from 300 K to 590 K. Overall, the resistivity $\rho$ of all the samples decreases monotonically with increasing temperature, showing non-degenerate semiconducting behavior. Nevertheless, $\rho$ of the Cu-doped samples is much smaller than that of the undoped $Bi_2Se_3$ sample. For instance, the resistivity $\rho$ of the un-doped $Bi_2Se_3$ sample decrease from $3.97 \times 10^{-5}$ Ωm to $2.68 \times 10^{-5}$ Ωm with increasing temperature from 300 K to 590 K; while the lightly Cu-doped samples ($x < 0.020$) show a resistivity changing from 3.60–3.80 $\times 10^{-5}$ Ωm to 1.52–1.61 $\times 10^{-5}$ Ωm in the same temperature range. For the heavily doped sample $Cu_{0.02}Bi_2Se_3$, however, the resistivity decrease greatly and reaches $2.73 \times 10^{-5}$ Ωm and $1.34 \times 10^{-5}$ Ωm at 300 K and 590 K, respectively, which could be related to its larger orientation factor ($\gamma = 0.33$) than the more lightly doped samples, besides the doping effect.

The temperature dependences of the Seebeck coefficient S for the $Cu_xBi_2Se_3$ samples ($x = 0$, 0.005, 0.010, 0.015 and 0.020) is depicted in Fig. 5. The negative values of the Seebeck coefficient found for all samples over the entire temperature range show that the major charge carriers in $Cu_xBi_2Se_3$ are electrons. For all Cu-doped samples, the absolute values of the Seebeck coefficient, $|S|$, decrease with increasing temperature, reflecting their non-degenerate behavior, which is in agreement with the behavior of the electrical resistivity $\rho$ (Fig. 4). In comparison, $|S|$ of the doped samples is substantially smaller than that of the un-doped one: $|S|$ of the undoped sample $Bi_2Se_3$ decrease from 178 μV/K to 140 μV/K as $T$ increase from 300 K to 590 K while $|S|$ of $Cu_xBi_2Se_3$ ($x = 0.005$, 0.010, 0.015 and 0.020) decrease rapidly from 170 μV/K to 105 μV/K as T increase from 300 K to 550 K. $|S|$ of the doped samples re increases slightly with further increasing $T$. The overall decrease in $|S|$ of the doped samples can be ascribed to the increase in electron concentration $n$ upon Cu doping. According to Mott's formula, the thermopower $S$ can be expressed as:

$$S = \frac{\pi^2 k_B^2 T}{3n}\left[\frac{\partial \ln(\sigma(E))}{\partial E}\right]_{E=E_f} = \frac{\pi^2 k_B^2 T}{3e}\left[\frac{1}{n}\frac{\partial n(E)}{\partial E} + \frac{1}{\mu}\frac{\partial \mu(E)}{\partial E}\right]_{E=E_f} \quad (1)$$

where $e$ is electron charge, $\mu(E)$ the electron mobility, $k_B$ the Boltzmann constant, and $E_f$ is the Fermi energy. Eq. (1) indicates

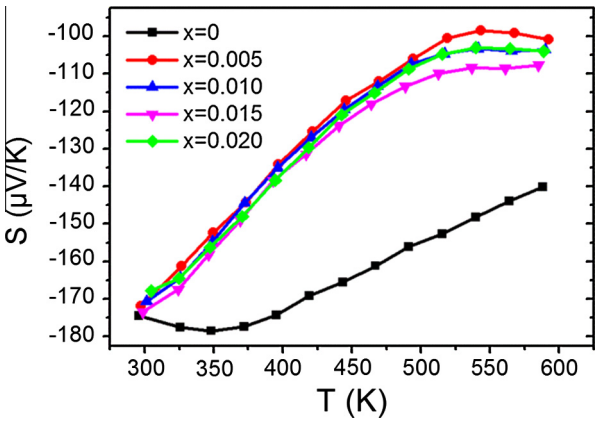


**Fig. 5.** Temperature dependences of Seebeck coefficient S for the $Cu_xBi_2Se_3$ ($x = 0$, 0.005, 0.010, 0.015 and 0.020) samples.

that $|S|$ decreases with increasing $n$, which can also explain why $|S|$ decreases with increasing doping content for the lightly doped samples ($x = 0.005$–$0.015$). However, $|S|$ of the sample for $x = 0.020$ increases again and is comparable to that of the sample for $x = 0.010$. A similar behavior was reported in $(Zn_{0.992}Al_{0.008}O)_mIn_2O_3$ [36]. This unusual re increase in $|S|$ for the sample with $x = 0.020$ could be caused by an increase in the scattering parameter $\lambda$, We rewrite the Eq. (1) as

$$S = \frac{\pi^2 k_B^2 T}{3e}\left[\frac{1}{n}\frac{\partial n(E)}{\partial E} + \frac{\lambda - \frac{1}{2}}{E}\right]_{E=E_f} \quad (2)$$

with $\mu = q\tau/m^*$ where $q$, $\tau$ and $m^*$ are the electron charge, relaxation time, and effective mass, respectively (here we assume that the relaxation time follows a power law in energy $\tau = \tau_0 E^{(\lambda-1/2)}$). Obviously, as the doping content increases the number of ionized impurities (dopants) should increase, which will cause the carrier scattering mechanism to transform from acoustic-dominant phonon scattering ($\lambda = 0$) to ionized impurity-dominated scattering ($\lambda = 2$), giving rising to an enhancement of the thermopower, as seen in Fig. 5.

Obviously, the increase in $n$ in the doped samples also explains why their resistivity $\rho$ is decreased as compared to that of the undoped sample since $\rho = 1/ne\mu$. This increased electron concentration $n$ could be caused by the above discussed intercalation of Cu into the van der Waals layers of $Bi_2Se_3$, for the doping of any guest

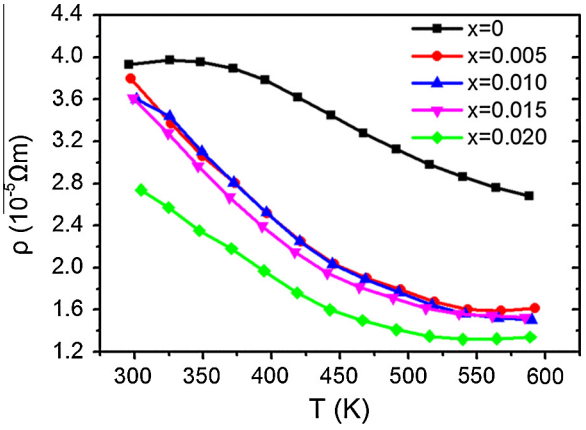


**Fig. 4.** Temperature dependences of resistivity $\rho$ for the $Cu_xBi_2Se_3$ ($x = 0$, 0.005, 0.010, 0.015 and 0.020) samples.

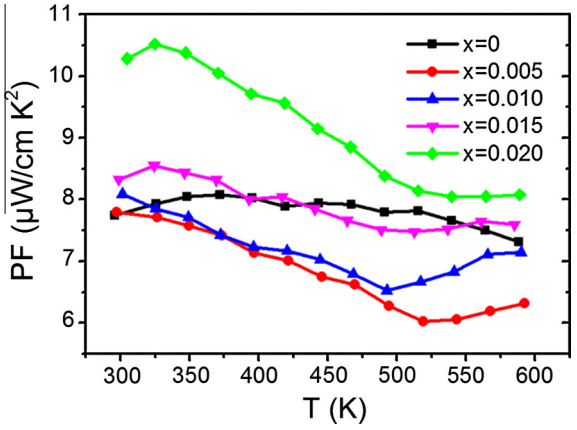


**Fig. 6.** Temperature dependences of power factor PF for the $Cu_xBi_2Se_3$ ($x = 0$, 0.005, 0.010, 0.015, 0.020) samples.

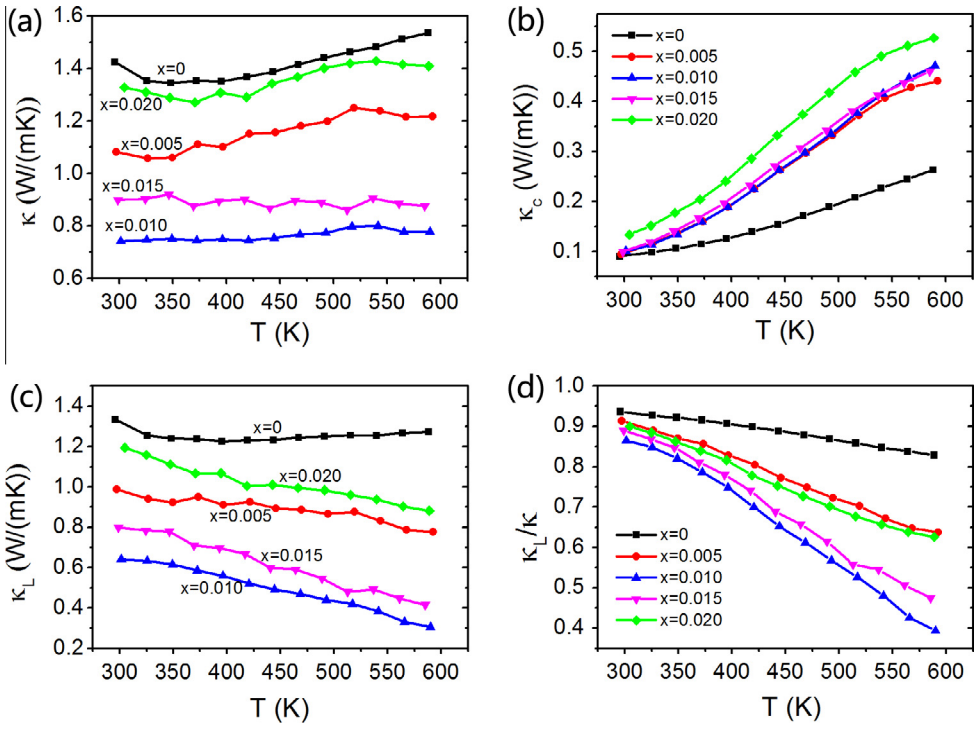


**Fig. 7.** Total thermal conductivity κ (a), carrier thermal conductivity $\kappa_c$ (b), lattice thermal conductivity $\kappa_L$ (c), and ratio of lattice to total thermal conductivity $\kappa_L/\kappa$ (d) of the $Cu_xBi_2Se_3$ ($x = 0$, 0.005, 0.010, 0.015 and 0.020) samples.

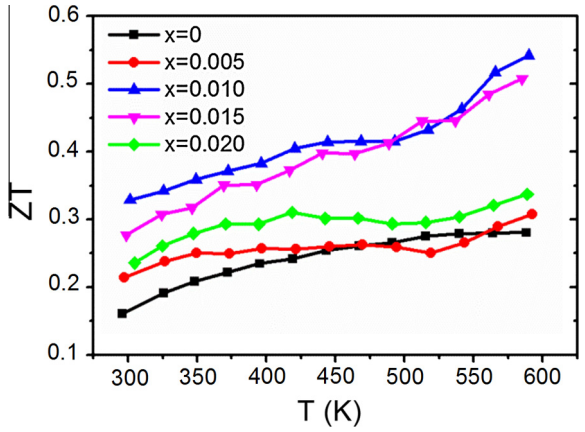


**Fig. 8.** Temperature dependences of figure of merit ZT for the $Cu_xBi_2Se_3$ ($x = 0$, 0.005, 0.010, 0.015 and 0.020) samples.

atom in van der Waals layers reproves interstitial doping and thus to donor behaviors.

Fig. 6 shows the power factor PF as a function of temperature. PF changes systematically with the Cu content. Although the PF of most of the doped sample is not larger than that of the undoped sample, the PF of the heavily doped sample $Cu_{0.02}Bi_2Se_3$ is substantially larger than that of the un-doped one, and has the largest PF with a peak value reaching ~10.5 μW cm$^{-1}$ K$^{-2}$ at ~325 K, which is mainly due to its low resistivity ρ (see Fig. 4).

### 3.3. Thermal conductivity and thermoelectric performance

The total thermal conductivity κ of all $Cu_xBi_2Se_3$ samples ($x = 0.005$, 0.010, 0.015 and 0.020) is given in Fig. 7(a). κ of the samples increases slightly with increasing temperature. Cu-doping causes a large reduction of κ with respect to the undoped sample. As shown in Fig. 7(a), κ = 1.35–1.54 W/mK for the undoped sample $Bi_2Se_3$ but only about 0.7–0.8 W/mK for $x = 0.010$. With further increasing Cu content, κ increase again. The lattice thermal conductivity $\kappa_L$ can be obtained from $\kappa = \kappa_L + \kappa_c$, in which $\kappa_c$ is the charge carrier contribution, which can be estimated by using the Wiedemann–Franz law: $\kappa_c = LT/\rho$, where $L$ is the Lorenz number. Here, $L = 1.5 \times 10^{-8}$ V$^2$ K$^{-2}$ is used, for this value is widely used in low-dimensional materials and nondegenerate semiconductors [37]. As shown in Fig. 7(b), the carrier thermal conductivity $\kappa_c$ for all the samples increases monotonically with increasing temperature due to the increased carrier concentration arising from thermal excitation at higher temperatures. $\kappa_c$ of the doped samples is obviously larger than that of the un-doped sample, which is attributed to the increased electron concentration of the doped samples in contrast to the mechanism that causes changes of $\kappa_c$ in p-type $Bi_{0.5}Sb_{1.5}Te_3$ [38,39]. Comparing Fig. 7(a) with Fig. 7(c) one finds that although κ and $\kappa_L$ show similar trends as function of the doping content $x$, they have different temperature dependences. That is, κ increases slightly with increasing temperature while $\kappa_L$ decreases with increasing temperature due to enhanced phonon–phonon scattering. Obviously, the increase of κ with temperature is caused by the temperature dependence of $\kappa_c$, as shown in Fig. 7(b). Likewise, the enhanced contribution of $\kappa_c$ can explain why $\kappa_L/\kappa$ for all the samples decreases with increasing temperature and why $\kappa_L/\kappa$ is smaller for the doped samples $Cu_xBi_2Se_3$ ($x = 0.005$, 0.010, 0.015 and 0.020) than for the un-doped sample (Fig. 7(d)).

As is well known, besides doping the lattice thermal conductivity $\kappa_L$ can be influenced by microstructural factors, such as porosity (or relative density), grain size, or preferred orientation. As shown in Table 1, the differences of the porosity, grain size, and preferred orientation (orientation factor γ) in the samples with different Cu contents are not very large. In other words, the changes (decreases) of $\kappa_L$ of the $Cu_xBi_2Se_3$ samples with different Cu contents could be mainly caused by the copper doping. Since the van der Waals gaps

of $Bi_2Se_3$ have very large spaces, as Cu atoms are introduced only weak chemical bonds between Cu and Se can be formed. This means that the doped Cu atoms can vibrate with low frequencies, or "rattle" in the doped sites as filled-atoms do in $CoSb_3$ [40–42], leading to strong phonon scattering or even to a modified phonon density of states. This can explain why $\kappa_L$ of the $Cu_xBi_2Se_3$ samples decrease remarkably as the Cu content $x$ increases from $x = 0$ to $x = 0.010$ (as shown in Fig. 7(c)). However, with further increasing the Cu content to $x = 0.015$ and 0.020, $\kappa_L$ increases again. This increase in $\kappa_L$ for the heavily doped samples could be caused by the formation of stronger bonding between doped Cu atoms and neighboring Se atoms of the host or/and by an ordered distribution of Cu atoms in the gaps upon heavy doping, both of which tend to weaken the phonon scattering.

Fig. 8 shows temperature dependences of ZT for all the samples. ZT of all Cu doped samples is larger than that of the undoped sample. This result indicates that Cu doping is an effective way to the enhancement of thermoelectric performance for $Bi_2Se_3$. The ZT values of the samples with $x = 0.01$ and 0.015 are substantially larger than that of the un-doped sample reaching a maximum value of ~0.54 at about 590 K due to the large reduction of $\kappa_L$ by Cu doping. Notably, the largest value of ZT obtained here (ZT = 0.54) is substantially larger than all the values (ZT = 0.096–0.35) reported for $Bi_2Se_3$ [23–26].

## 4. Conclusions

In summary, we have investigated the thermoelectric properties of the Cu-doped $Cu_xBi_2Se_3$ ($x = 0$, 0.005, 0.010, 0.015 and 0.020) samples in the temperature range of 300 K to 590 K. Our study shows that the thermoelectric properties of the Cu-doped samples is sizably enhanced as compared to un-doped $Bi_2Se_3$. The electrical resistivity $\rho$ is decreased by about 30% at 500 K upon doping. Although the power factor PF for most of the doped samples is not superior to that of the un-doped $Bi_2Se_3$, $\kappa_L$ of the moderately doped samples with $x = 0.01$ and 0.015 is strongly reduced (by 30–50% at 300 K) presumably due to enhanced phonon scattering of the dopant. As a result, ZT of all the doped samples is enhanced as compared with that of the un-doped samples, and the largest value of ZT = 0.54 at 590 K is obtained for $Cu_{0.01}Bi_2Se_3$.

## Acknowledgements

Financial support from the National Natural Science Foundation of China (Nos. 11174292, 11374306, 51101150) and from the Austrian Science Found (FWF Project TRP 176-N22) are gratefully acknowledged.

## References

[1] Y. Zhang, X. Jia, L. Deng, X. Guo, H. Sun, B. Sun, B. Liu, H. Ma, J. Alloys Comp. 632 (2015) 514–519.
[2] X.a. Fan, Z. Rong, F. Yang, X. Cai, X. Han, G. Li, J. Alloys Comp. 630 (2015) 282–287.
[3] P.H. Le, C.-N. Liao, C.W. Luo, J. Leu, J. Alloys Comp. 615 (2014) 546–552.
[4] T.H. Zou, X.Y. Qin, D. Li, L.L. Li, G.L. Sun, Q.Q. Wang, J. Zhang, H.X. Xin, Y.F. Liu, C.J. Song, J. Alloys Comp. 588 (2014) 568–572.
[5] J. Zhang, X.Y. Qin, D. Li, H.X. Xin, C.J. Song, L.L. Li, Z.M. Wang, G.L. Guo, L. Wang, J. Alloys Comp. 586 (2014) 285–288.
[6] H.R. Williams, R.M. Ambrosi, K. Chen, U. Friedman, H. Ning, M.J. Reece, M.C. Robbins, K. Simpson, K. Stephenson, J. Alloys Comp. 626 (2015) 368–374.
[7] Q. Lognoné, F. Gascoin, J. Alloys Comp. 610 (2014) 1–5.
[8] J.-E. Hong, S.-K. Lee, S.-G. Yoon, J. Alloys Comp. 583 (2014) 111–115.
[9] S.J. Kim, J.H. We, J.S. Kim, G.S. Kim, B.J. Cho, J. Alloys Comp. 582 (2014) 177–180.
[10] C.M. Kim, S.H. Kim, T. Onimaru, K. Suekuni, T. Takabatake, M.H. Jung, Curr. Appl. Phys. 14 (2014) 1041–1044.
[11] Y. Saeed, N. Singh, U. Schwingenschlögl, Appl. Phys. Lett. 105 (2014) 031915.
[12] J. Laopaiboon, S. Pencharee, T. Seetawan, U. Patakham, B. Chayasombat, C. Thanachayanont, Mater. Lett. 141 (2015) 307–310.
[13] A. Kadhim, A. Hmood, H.A. Hassan, Mater. Sci. Semicond. Process. 26 (2014) 379–387.
[14] H.-S. Kim, S.-J. Hong, J. Alloys Comp. 586 (Supplement 1) (2014) S428–S431.
[15] G.E. Lee, I.H. Kim, Y.S. Lim, W.S. Seo, B.J. Choi, C.W. Hwang, J. Korean Phys. Soc. 64 (2014) 1416–1420.
[16] H.S. Kim, S.J. Hong, Curr. Nanosci. 10 (2014) 118–122.
[17] D. Bourgault, B. Schaechner, C. Giroud Garampon, T. Crozes, N. Caillault, L. Carbone, J. Alloys Comp. 598 (2014) 79–84.
[18] V.B. Osvenskiy, V.P. Panchenko, Y.N. Parkhomenko, A.I. Sorokin, D.I. Bogomolov, V.T. Bublik, N.Y. Tabachkova, J. Alloys Comp. 586 (Supplement 1) (2014) S413–S418.
[19] S. Jimenez, J.G. Perez, T.M. Tritt, S. Zhu, J.L. Sosa-Sanchez, J. Martinez-Juarez, O. López, Energy Convers. Manage. 87 (2014) 868–873.
[20] O.A. Tretiakov, A. Abanov, J. Sinova, Appl. Phys. Lett. 99 (2011) 113110.
[21] L. Muchler, F. Casper, B.H. Yan, S. Chadov, C. Felser, Phys. Status Solidi RRL 7 (2013) 91–100.
[22] D. Kim, P. Syers, N.P. Butch, J. Paglione, M.S. Fuhrer, Nano Lett. 14 (2014) 1701–1706.
[23] K. Kadel, L. Kumari, W.Z. Li, J.Y. Huang, P.P. Provencio, Nanoscale Res. Lett. 6 (6) (2011) 57.
[24] Y.S. Hor, A. Richardella, P. Roushan, Y. Xia, J.G. Checkelsky, A. Yazdani, M.Z. Hasan, N.P. Ong, R.J. Cava, Phys. Rev. B 79 (2009) 195208.
[25] Y. Min, J.W. Roh, H. Yang, M. Park, S.I. Kim, S. Hwang, S.M. Lee, K.H. Lee, U. Jeong, Adv. Mater. 25 (2013) 1425–1429.
[26] Y. Sun, H. Cheng, S. Gao, Q. Liu, Z. Sun, C. Xiao, C. Wu, S. Wei, Y. Xie, J. Am. Chem. Soc. 134 (2012) 20294–20297.
[27] S. Nakajima, J. Phys. Chem. Solids 24 (1963) 479–485.
[28] J. Zhang, X.Y. Qin, H.X. Xin, D. Li, C.J. Song, J. Electron. Mater. 40 (2011) 980–986.
[29] M.S. Whittingham, Prog. Solid State Chem. 12 (1978) 41–99.
[30] D. Li, X.Y. Qin, J. Zhang, H.J. Li, Phys. Lett. A 348 (2006) 379–385.
[31] D. Li, X.Y. Qin, Y.J. Gu, Mater. Res. Bull. 41 (2006) 282–290.
[32] Y.S. Hor, A.J. Williams, J.G. Checkelsky, P. Roushan, J. Seo, Q. Xu, H.W. Zandbergen, A. Yazdani, N.P. Ong, R.J. Cava, Phys. Rev. Lett. 104 (2010) 057001.
[33] C. Mann, D. West, I. Miotkowski, Y.P. Chen, S. Zhang, C.-K. Shih, Phys. Rev. B 89 (2014) 155312.
[34] X. Luo, M.B. Sullivan, S.Y. Quek, Phys. Rev. B 86 (2012) 184111.
[35] F.K. Lotgering, J. Inorg. Nucl. Chem. 9 (1959) 113–123.
[36] K. Park, K.K. Kim, J.K. Seong, S.J. Kim, J.G. Kim, W.S. Cho, S. Nahm, Mater. Lett. 61 (2007) 4759–4762.
[37] X.B. Zhao, X.H. Ji, Y.H. Zhang, T.J. Zhu, J.P. Tu, X.B. Zhang, Appl. Phys. Lett. 86 (2005) 062111.
[38] K. Park, J.H. Seo, D.C. Cho, B.H. Choi, C.H. Lee, Mater. Sci. Eng. B 88 (2002) 103–106.
[39] K. Park, S.W. Nam, C.H. Lim, Intermetallics 18 (2010) 1744–1749.
[40] D. Li, K. Yang, H.H. Hng, Q.Y. Yan, J. Ma, T.J. Zhu, X.B. Zhao, J. Phys. D: Appl. Phys. 42 (2009) 105408.
[41] D. Li, K. Yang, H.H. Hng, X.Y. Qin, J. Ma, J. Appl. Phys. 104 (2008) 103720.
[42] S. Pailhes, H. Euchner, V.M. Giordano, R. Debord, A. Assy, S. Gomes, A. Bosak, D. Machon, S. Paschen, M. de Boissieu, Phys. Rev. Lett. 113 (2014) 025506.